Original Article

MOLECULAR METABOLISM

Antagonistic epistasis of Hnf4α and FoxO1 metabolic networks through enhancer interactions in β-cell function

Taiyi Kuo [1,*,4], Wen Du [1], Yasutaka Miyachi [1], Prasanna K. Dadi [2], David A. Jacobson [2], Daniel Segrè [3], Domenico Accili [1]

ABSTRACT

Objective: Genetic and acquired abnormalities contribute to pancreatic β-cell failure in diabetes. Transcription factors Hnf4α (MODY1) and FoxO1 are respective examples of these two components and act through β-cell-specific enhancers. However, their relationship is unclear.
Methods: In this report, we show by genome-wide interrogation of chromatin modifications that ablation of FoxO1 in mature β-cells enriches active Hnf4α enhancers according to a HOMER analysis.
Results: To model the functional significance of this predicted unusual enhancer utilization, we generated single and compound knockouts of FoxO1 and Hnf4α in β-cells. Single knockout of either gene impaired insulin secretion in mechanistically distinct fashions as indicated by their responses to sulfonylurea and calcium fluxes. Surprisingly, the defective β-cell secretory function of either single mutant in hyperglycemic clamps and isolated islets treated with various secretagogues was completely reversed in double mutants lacking FoxO1 and Hnf4α. Gene expression analyses revealed distinct epistatic modalities by which the two transcription factors regulate networks associated with reversal of β-cell dysfunction. An antagonistic network regulating glycolysis, including β-cell "disallowed" genes, and a synergistic network regulating protocadherins emerged as likely mediators of the functional restoration of insulin secretion.
Conclusions: The findings provide evidence of antagonistic epistasis as a model of gene/environment interactions in the pathogenesis of β-cell dysfunction.

Keywords Beta cell; Hnf4a; Foxo1; Enhancer; Insulin; Epistasis

1. INTRODUCTION

Genetic predisposition contributes to type 2 diabetes through changes in the expression and activity of transcription factors essential for β-cell function and insulin sensitivity [1]. The best characterized examples are MODY gene mutations, which generally act in an autosomal-dominant fashion to impair insulin secretion [2]. In the vast majority of patients, however, such predisposition is more subtle and requires acquired abnormalities often associated with altered nutrient utilization to cause overt β-cell dysfunction. An example of acquired transcriptional abnormalities leading to altered β-cell function is FoxO1, a nutrient-regulated transcription factor whose nutrient excess-driven failure leads first to metabolic inflexibility [3], and then to outright β-cell dedifferentiation [4–6]. This is achieved in part by direct actions on glucose metabolism [7] and in part by regulating lineage stability [8].

We were interested in exploring the functional relationship between FoxO1 and Hnf4α as a model of gene/environment interactions in the pathogenesis of β-cell dysfunction. When we ablated FoxO1, 3a, and 4 in pancreatic progenitors or mature β-cells, gene ontology analyses revealed that Hnf4α targets were the most altered [3]. However, whether these changes resulted in activation or repression of Hnf4α and whether they contributed to or offset FoxO1-induced β-cell dysfunction was not clear.

Mutations of *HNF4A* cause MODY1 [9]. Most patients develop diabetes in the third decade of life due to a primary defect in insulin secretion [10] that can be long-term treated with sulfonylureas [11]. In mice, pancreas-wide (Pdx1-*Cre*) or mature β-cell (Rip-*Cre*) deletion of Hnf4α causes glucose intolerance due to defective insulin secretion [12–14]. There are shared phenotypic features between FoxO-deficient and Hnf4α-deficient β-cells [3,12,14] that include compromised glucose-stimulated insulin secretion and altered Pparα and Hnf1α gene

[1]Department of Medicine and Berrie Diabetes Center, Columbia University College of Physicians and Surgeons, New York, NY, USA [2]Department of Molecular Physiology and Biophysics, Vanderbilt University, Nashville, TN, USA [3]Department of Biology, Department of Biomedical Engineering, Department of Physics, Boston University, Boston, MA, USA

[4] Lead Contact

*Corresponding author. Department of Medicine and Berrie Diabetes Center, Columbia University College of Physicians and Surgeons, 1150 St. Nicholas Avenue, Room 237, New York, NY, 10032, USA. E-mail: tk2592@cumc.columbia.edu (T. Kuo).

Received February 8, 2021 • Revision received May 4, 2021 • Accepted May 12, 2021 • Available online 25 May 2021

https://doi.org/10.1016/j.molmet.2021.101256

network expression indicative of shared pathways and targets of both transcription factors.

The present studies were undertaken to analyze a potential FoxO1/Hnf4α epistasis. Surveys of histone H3 lysine 27 acetylation for active promoters and enhancers uncovered an interplay between Hnf4α and FoxO1 at β-cell enhancers. Thus, we generated and compared mutant animals lacking FoxO1, Hnf4α, or both in β-cells. Surprisingly, FoxO1/Hnf4α double knockout mice (DKO) showed restored glucose tolerance and insulin secretion compared to single knockouts. These findings fundamentally change our understanding of the interactions within transcriptional networks regulating β-cell function by highlighting a heretofore unrecognized antagonistic epistasis [15].

2. RESEARCH DESIGN AND METHODS

2.1. Animals

We obtained Hnf4α flox/flox mice from Dr. Frank J. Gonzalez [14] and crossed Rip-*Cre*/*Rosa26-Tomato*/floxed *FoxO1* mice with floxed *Hnf4α* [8] to generate β-cell-specific FoxO1 and Hnf4α knockout mice. We categorized mice with at least one allele of FoxO1 and Hnf4α as WT for DKO studies [3]. The mice were on a mixed background and were littermates. Experiments were performed in 6- to 8-month-old male mice unless specified otherwise in the figure legends. All mice were fed chow diets and maintained on a 12-h light cycle (lights on at 7 am). Epigenetic screening was performed in female mice, and FoxO1 and Hnf4α double knockout validations were conducted in male mice.

2.2. Metabolic parameters

We performed intraperitoneal glucose tolerance tests with glucose (2 g/kg) after an overnight (16 h) fast and insulin tolerance tests by injecting insulin (0.75 units/kg) after a 5-h fast [16]. For hyperglycemic clamps, we followed a previously described protocol [7]. To assess insulin capacity in vivo, we raised the plasma glucose level to ∼350 mg/dL by continuous infusion of glucose and maintained it by adjusting the glucose infusion rate on the pump. Throughout the 120-min period, we recorded the glucose infusion rates and plasma glucose levels and collected plasma for insulin measurement. Metabolic features of NGT and DM mice are described in [8].

2.3. Fluorescence-assisted β-cell sorting

Pancreatic islets were isolated as described and allowed to recover in RPMI supplemented with 15% FBS overnight [16]. The next day, the islets were washed with PBS and dissociated with trypsin, followed by quenching with FBS. Thereafter, the dispersed islets were spun down, washed with PBS, and incubated with SYTOX Red (Thermo Fisher Scientific, S34859) to identify live cells and DNase I (Sigma, D4513) on ice until sorting. Prior to sorting, the cells were filtered through a 35-μm cell strainer (Corning, 352,235) to remove clusters. Tomato-positive and -negative cells differed by ∼2 orders of magnitude in Tomato fluorescence with excitation of 554 nm and emission of 581 nm by an Influx cell sorter (BD Biosciences).

2.4. H3K27ac ChIPseq

Islet β-cells were genetically labeled with ROSA26-Tomato fluorescence with Rip-*Cre* allele, and FAC-sorted β-cells were used for histone H3K27ac ChIPseq with anti-H3K27ac antibody (Active Motif, 39,133). ChIP and ChIPseq were performed as previously described [8,17]. The resulting DNA libraries were quantified with Bioanalyzer (Agilent) and sequenced on an Illumina NextSeq 500 with 75-nt reads and single ends. Reads were aligned to mouse genome mm10 using the Burrows-Wheeler Aligner (BWA) algorithm with default settings [18]. These reads passed Illumina's purity filter and aligned with no more than 2 mismatches. Duplicate reads were removed, and only uniquely mapped reads with a mapping quality greater or equal to 25 were subjected to further analysis. Alignments were extended in silico at their 3′ ends to a length of 200 bp, which is the average genomic fragment length in the size-selected library, and assigned to 32-nt bins along the genome. Peak locations were determined using the MACS algorithm (v1.4.2) with a cutoff of p value $= 1 \times 10^{-7}$ [19]. ROSE was used to identify enhancers [20].

2.5. Enhancer motif analysis

For H3K27ac ChIPseq, HOMER was used to create tag directories and call broad peaks. Cisgenome was used to find the distribution of H3K27ac peaks in the genome. We used a cutoff of +/− 3 kb from the TSS to separate enhancers and promoters. De novo motif analysis was done using HOMER in the troughs of differentially acetylated enhancers identified from H3K27ac. To compare peak metrics between samples, common intervals were categorized as active regions defined by the start coordinate of the most upstream interval and the end coordinate of the most downstream interval. Active regions also included those intervals found in only one sample. Tag density represented the DNA fragment per 32-bp bin. To generate scatterplots of H3K27ac in promoter or distal enhancer regions, the parameters for differential peak calling for all WT vs all IKO were as follows: fragments per kilobase of DNA per 10 million mapped reads (FPKTM) >10 for at least one of the groups, and fold change (FC) > 1.5. The parameters for differential peak calling for NGT vs DM were as follows: FPKTM > 30 for at least one of the groups, and FC > 1.5.

2.6. RNAseq

We isolated total RNA with a Nucleospin RNA kit (Macherey—Nagel) with DNase I treatment following a previously described protocol [21]. Directional poly-A RNAseq libraries were prepared and sequenced as PE42 (42-bp paired-end reads) on an Illumina NextSeq 500. For the analysis, 29 to 45 million read pairs per sample were used. The reads were mapped to the mouse genome mm10 using the STAR (v2.5.2b) [22] algorithm with default settings. FeatureCounts from the Subread (v1.5.2) [23] Package was used to assign concordantly aligned read pairs to RefSeq genes. A 25-bp minimum as overlapping bases in a fragment was specified for read assignment. Raw read counts were used as input for DESeq2 (v1.14.1) [24], which was used to filter out genes with low counts, normalize the counts using library sizes, and perform statistical tests to find significant differential genes. The differential calling results are presented in Supplemental Tables S1—6. For statistical analysis, a cutoff of p value < 0.05 and FDR < 0.1 was applied, and the resulting genes were used as input for gene ontology analyses (Ingenuity Pathway Analysis software, Qiagen). Raw and processed data were deposited into the MINSEQE-compliant National Center for Biotechnology Information Gene Expression Omnibus database.

2.7. Epistasis analysis

To obtain the modality of epistasis between FoxO1 and Hnf4α, we first calculated the average FPKM for the 5 replicates from RNAseq followed by the normalization of IKO, HKO, and DKO to WT. We then used the following equation: epistasis (ε) = R observed (DKO) - R expected (IKO + HKO). Then a two-standard deviations cutoff was applied to assign genes as synergistic, non-epistatic, or antagonistic (Supplemental Table S7). DAVID (https://david.ncifcrf.gov/home.jsp) was used for the gene ontology analysis.

2.8. Fura-2 AM imaging of whole-islet secretagogue-stimulated calcium influx

Purified islets were loaded with 2 μM of Fura-2 acetoxymethyl ester (AM) for 25 min at 37 °C with 5% CO_2. Islets were washed twice with Krebs buffer and incubated in Krebs buffer supplemented with 2 mM of glucose for 20 min to reach basal conditions before imaging. Then 14 mM of glucose and 45 mM of KCl were added sequentially to stimulate calcium flux. Relative intracellular calcium concentrations were measured every 5 s as a ratio of Fura-2 fluorescence excitation at 340 and 380 nm (F340/F380) both with 510 nm emission using a Nikon Ti2 microscope equipped with a Photometrics Prime 95B camera followed by data analysis using Nikon Element software [25].

2.9. Statistics

Two-tailed Student's t-tests and ANOVA were performed with Prism (GraphPad) for quantitative PCR experiments, glucose tolerance tests, hyperglycemic clamp studies, and secretagogue-stimulated insulin secretion.

2.10. Study approval

The Columbia University Institutional Animal Care and Utilization Committee approved all of the experiments.

2.11. Data sharing and availability

We deposited all of the raw and processed ChIP and RNA sequencing data into the MINSEQE-compliant National Center for Biotechnology Information Gene Expression Omnibus database with accession number GSE161028.

3. RESULTS

3.1. Altered enhancer selection in β-cell failure

Activation of FoxO1 enhancers is a key event in β-cells in response to insulin-resistant diabetes in *db/db* mice [7]. We investigated FoxO1-regulated enhancers in a multiparity model of diabetes associated with genetic ablation of FoxO1 [4,8]. To this end, we subjected fluorescently sorted β-cells from 12-month-old multiparous diabetic β-cell-specific FoxO1 knockout mice (multiparous IKO or DM) and glucose-tolerant controls (multiparous WT, normal glucose tolerance, or NGT) [8] to genome-wide chromatin immunoprecipitation with acetylated histone 3 lysine 27 antibodies (H3K27ac) as a marker of active enhancers and promoters [26]. DM mice showed evidence of multiparity-associated β-cell failure with random and refed hyperglycemia as well as fasting and refed hypoinsulinemia [4,8]. We observed a global increase in H3K27ac in active regions (Fig. S1A) and individual genes (Fig. S1B) of DM β-cells. Nearly half (44%) of H3K27ac peaks were located in introns, 14% in intergenic regions, and 16% in promoters (Fig. S1C). We analyzed the data based on H3K27ac regions associated with promoters (defined as +/− 3 kb from transcription start sites) or distal enhancers (defined as beyond promoters) [27]. Interestingly, we detected significant changes in distal enhancers in the absence of FoxO1 as opposed to promoters regardless of age or parity (Figure 1A,B). Specifically, across all three comparisons of 12-month-old multiparous WT (NGT) vs IKO (DM), 12-month-old nulliparous (12M NP) WT vs IKO, and 3-month-old nulliparous (3M) WT vs IKO β-cells (all WT vs all IKO), there were 417 hyper-acetylated and 149 hypo-acetylated distal enhancers (Figure 1A). In contrast, we found minimal alterations in the promoters (Figure 1B). As such, we found 31 hyper-acetylated and 15 hypo-acetylated promoters across all three comparisons (Figure 1B). These data confirmed the importance of FoxO1 in distal enhancers [7].

To investigate the functional consequences of the altered distal enhancer profile of all WT vs all IKO, we mined transcription factor-binding motifs associated with each of the two categories: hyper-acetylated and hypo-acetylated enhancers. We hypothesized that activation of transcription factors would be associated with enrichment of the relevant motifs in hyper-acetylated enhancers, whereas suppression of transcription factors would be associated with enrichment of their motifs in hypo-acetylated enhancers [7]. Among the hyper-acetylated motifs, we found Nkx2.5, Hnf4α, Isl1, Pitx, and Irf. In contrast, among the hypo-acetylated motifs, we found Hox, FoxO1, and Sox (Figure 1C).

We then focused on comparing NGT vs DM β-cell distal enhancers. With a more stringent parameter of increased FPKM requirements, we found 343 hyper-acetylated and 116 hypo-acetylated distal enhancers (Figure 1D). We then mined transcription factor-binding motifs associated with each category. Consistently, FoxO1 was the second most over-represented motif found within the hypo-acetylated enhancers in all IKO and DM β-cells, further validating the analysis (Figure 1E). We also found a significant depletion of the Pax6 motif, a FoxO1 target [28,29] that regulates *Ins1*, *Ins2* [30], Nkx6.1, Pdx1, Slc2a2, and Pc1/3 in β-cells [31]. Pax6 represses alternative islet cell genes including ghrelin, glucagon, and somatostatin [32], and ablation of Pax6 in the adult pancreas leads to glucose intolerance due to β-cell dedifferentiation [31,32]. The data were consistent with the possibility that combined abnormalities of FoxO1 and Pax6 contribute to β-cell dedifferentiation.

In contrast, Hnf4α was the top hyper-acetylated motif shared in common by all IKO and DM β-cells (Figure 1E). This finding was consistent with prior gene ontology analyses indicating activation of the Hnf4α network in triple FoxO [3] and single FoxO1 knockout β-cells [8]. In addition, Hic [33] and Ets [34], two networks of potential interest for β-cell stability, were over-represented. Interestingly, Ets1 overexpression in β-cells suppresses insulin secretion [35]. These data reveal a striking rearrangement of active enhancers in diabetic β-cells.

3.2. Restoration of metabolic parameters in FoxO1 and Hnf4α double knockout mice

The over-representation of Hnf4α enhancers together with prior RNAseq data [3,8,36] led us to ask whether changes in Hnf4a function are compensatory or contributory vis-à-vis β-cell dysfunction. To this end, we generated β-cell-specific FoxO1 (IKO), Hnf4α (HKO) [14], and double knockout (DKO) mice using Rip-*Cre* transgenic mice [37] that do not cause extra-pancreatic recombination or produce Gh mRNA [38]. The animals were born to term in the expected Mendelian ratios and showed no growth abnormalities (Fig. S2A).

We performed oral glucose tolerance tests. As previously reported, IKO or HKO mice displayed glucose intolerance (Figure 2A) [4,8,12,14]. Unexpectedly, compared to single knockouts, the DKO mice showed restoration of normal glucose tolerance (Figure 2A,B). We also assessed plasma glucose levels within 5 min of intraperitoneal glucose injection as a surrogate measure of insulin secretion. Consistent with the glucose tolerance tests, the IKO mice showed elevated glucose levels within 5 min, whereas the DKO mice showed no difference compared to WT (Figure 2C). To investigate the nutrient response, we measured glucose and insulin levels in fasted and refed mice. While no difference was found in fasted plasma glucose and insulin levels between all 4 genotypes, refeeding led to elevated plasma glucose and reduced insulin levels in the IKO mice compared to WT (Figure 2D,E). Interestingly, the DKO and WT mice showed similar levels of glucose and insulin in response to a meal (Figure 2D,E).

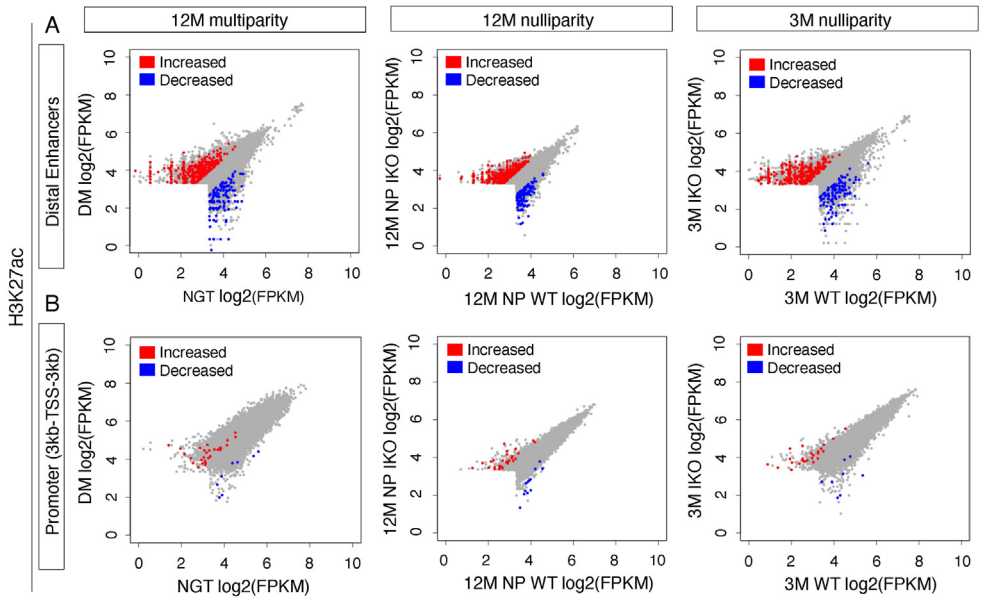

C

Transcription factor motif analysis for all WT *vs.* all IKO H3K27ac distal enhancers

Hyper-acetylated motifs		Hypo-acetylated motifs	
Homer top 5 *de novo* motifs	Significance	Homer top 3 *de novo* motifs	Significance
TACAGGCTCTCA	Nkx2.5 *p* value 1 x 10^{-13}	AGCTTTACTACA	Hox *p* value 1 x 10^{-13}
TTGGGCTATAGG	Hnf4α *p* value 1 x 10^{-13}	ATCAAACATATA	Foxo1 *p* value 1 x 10^{-13}
CTCCTATTAGGG	Isl1 *p* value 1 x 10^{-12}	TAATTGTGCC	Sox *p* value 1 x 10^{-12}
AAGGGGAGTA	Pitx *p* value 1 x 10^{-12}		
ACTAAATGAAAG	Irf *p* value 1 x 10^{-12}		

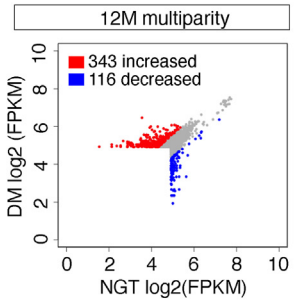

E

Transcription factor motif analysis for NGT *vs.* DM H3K27ac distal enhancers

Hyper-acetylated motifs		Hypo-acetylated motifs	
Homer top 5 *de novo* motifs	Significance	Homer top 5 *de novo* motifs	Significance
GAGGGACTAAAG	Hnf4α *p* value 1 x 10^{-21}	TGAATAATTG	Pax6 *p* value 1 x 10^{-12}
CTGTGCCCTTTC	Hic *p* value 1 x 10^{-19}	GCAAGCCTGTTT	FoxO1 *p* value 1 x 10^{-11}
AGGAAACTGGAT	Ets *p* value 1 x 10^{-17}	TATGTAACTGAG	Rfx *p* value 1 x 10^{-11}
GCCACGCGTCGT	Hes1 *p* value 1 x 10^{-17}	CCTTCCCCTGTA	Tead1 *p* value 1 x 10^{-11}
ACCTACGCCC	Klf *p* value 1 x 10^{-16}	CGGATGGTCTCT	Prdm14 *p* value 1 x 10^{-11}

Figure 1: Motif analysis of distal enhancers. (A–B) Scatterplots of H3K27ac regions in distal enhancers (A) and promoters (B) in WT and β cell-specific Foxo1 knockout (IKO) β-cells isolated under three conditions: 12-month-old (12M) female diabetic multiparous IKO (DM) and WT controls (multiparous WT, normal glucose tolerance, or NGT), age-matched female nulliparous (12M NP) IKO and WT controls, and 3-month-old female nulliparous (3M NP) IKO and WT controls. Across all three comparisons (all WT vs all IKO), there were 417 upregulated (red) and 149 downregulated (blue) H3K27ac regions in distal enhancers (A) and 31 upregulated (red) and 15 downregulated (blue) H3K27ac regions in promoters (B). For A and B, the parameters for differential peak calling for all WT vs all IKO were as follows: fragments per kilobase of DNA per 10 million mapped reads (FPKTM) $>$ 10 for at least one of the groups, and Fold Change (FC) $>$ 1.5. (C) Transcription factor HOMER motif analysis performed separately in hyper-acetylated (red in A) or hypo-acetylated (blue in A) distal enhancers. The top de novo motifs and *p* values are shown. (D) For NGT *vs* DM distal enhancers, a more stringent parameter for differential peak calling was applied: FPKTM $>$30 for at least one group, and FC $>$ 1.5. There were 343 upregulated (red) and 116 downregulated (blue) distal enhancers. (E) Transcription factor HOMER motif analysis performed separately in hyper-acetylated (red in D) or hypo-acetylated (blue in D) distal enhancers. The top de novo motifs and *p* values are shown.

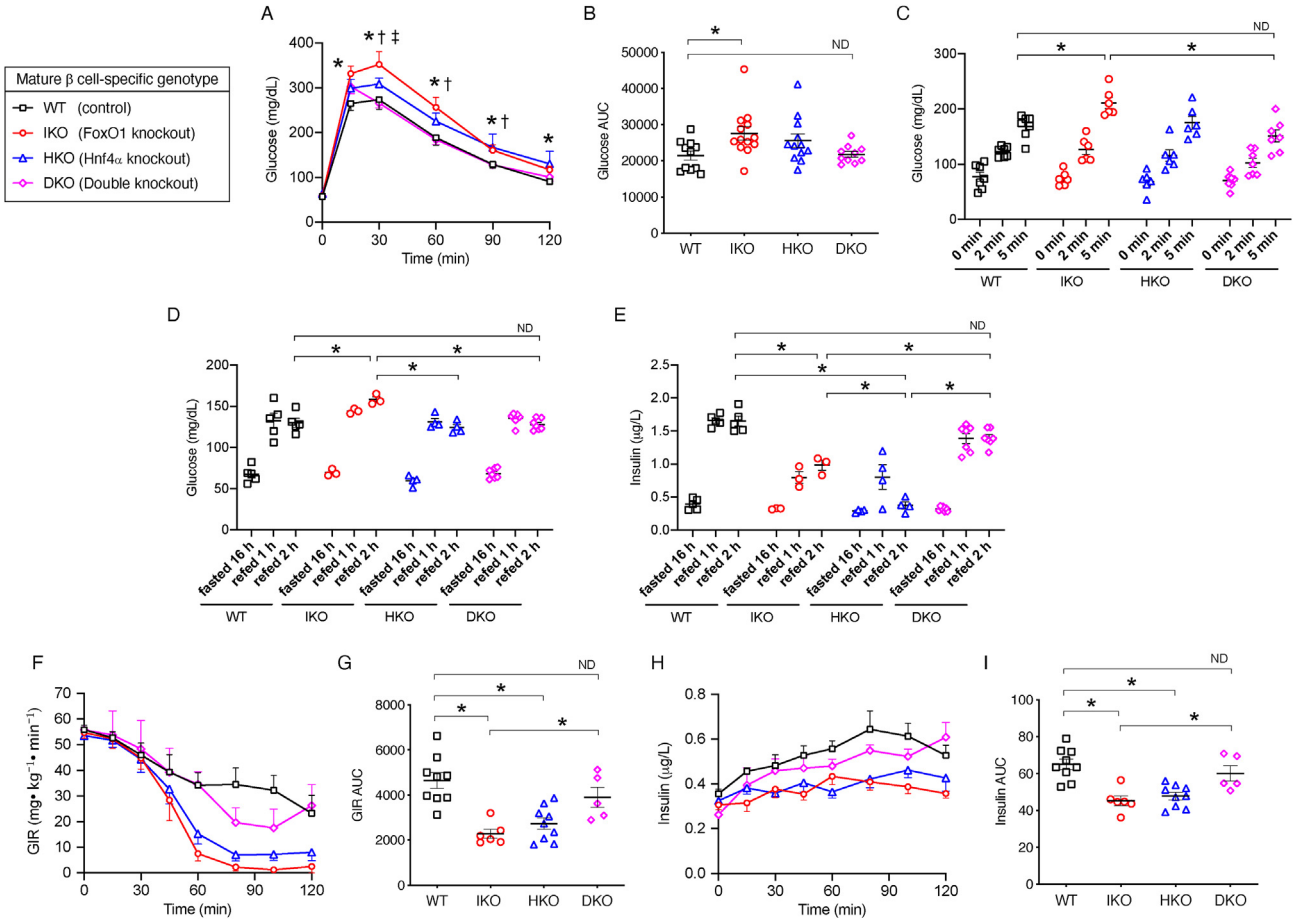

Figure 2: Glucose tolerance tests, fasting and refeeding response, and hyperglycemic clamps. (A) Intraperitoneal glucose tolerance test in WT (n = 11), IKO (n = 13), HKO (n = 12), and DKO (n = 10) mice. † represents $p < 0.05$ for IKO vs DKO, * indicates $p < 0.05$ for WT vs IKO, and ‡ shows $p < 0.05$ for HKO vs DKO. (B) Area under the curve (AUC) in A. Error bars represent SEM, $*p < 0.05$ using Student's t-test and ANOVA. (C) Glucose levels in WT (n = 7), IKO (n = 6), HKO (n = 5), and DKO (n = 7) mice within 5 min of intraperitoneal glucose injection. (D–E) Glucose (D) and plasma insulin levels (E) in fasted or refed WT (n = 5), IKO (n = 3), HKO (n = 4), and DKO (n = 5) mice. (F) Glucose infusion rates (GIRs) during hyperglycemic clamps in WT (n = 9), IKO (n = 6), HKO (n = 9), and DKO (n = 5) mice and (G) quantification of AUC. Error bars represent SEM, $*p < 0.05$ using Student's t-test and ANOVA. (H) Circulating insulin levels during hyperglycemic clamps in WT (n = 9), IKO (n = 6), HKO (n = 9), and DKO (n = 5) mice and (I) quantification of AUC. Error bars represent SEM, $*p < 0.05$ using Student's t-test and ANOVA. ND stands for no difference.

To assess insulin secretory capacity in vivo, we used hyperglycemic clamps. Via intravenous glucose administration, we raised glycemia to ~350 mg/dL (Figs. S2B and S2C) and measured the rate of glucose infusion necessary to maintain this level. The DKO mice showed increased glucose infusion rates compared to the IKO and HKO to a level indistinguishable from WT (Figure 2F,G). Plasma insulin levels increased accordingly, consistent with an improved insulin secretory capacity in the DKO mice (Figure 2H,I). In contrast, all 4 genotypes responded to exogenous insulin injection to a comparable extent (Fig. S2D). These data were consistent with the possibility that FoxO1 and Hnf4α have antagonistic epistasis on the phenotype of insulin secretion in β-cells, and that Hnf4α over-representation in hyper-acetylated enhancers in the absence of FoxO1 contributes to β-cell dysfunction.

3.3. Secretagogue-stimulated insulin secretion and calcium flux

To investigate the mechanism of restored insulin secretion, we subjected purified islets from all four genotypes to insulin secretion in response to various secretagogues. Consistent with the in vivo studies, IKO and HKO islets showed impaired insulin secretion in response to high glucose or arginine, which was restored to WT levels in DKO islets (Figure 3A,B). Similar to studies in triple FoxO knockout islets, IKO islets also showed compromised insulin secretion in response to the sulfonylurea glibenclamide and the PKC activator PMA [3]. Both responses were normal in HKO and restored in DKO islets (Figure 3C,D). Although the sulfonylurea response differed from previously reported data in Hnf4α knockout β-cells [12,14], it was consistent with the clinical response of MODY1 patients [11].

To probe the amplifying signal in insulin secretion, we tested exendin-4, a GLP-1 agonist, and GIP treatment. We found that both exendin-4- and GIP-stimulated insulin secretion were comparable in WT, IKO, and DKO islets (Figure 3E,F), indicating that the GLP-1 and GIP receptor-dependent pathways of insulin secretion were not affected by FoxO1 ablation. It was shown that GLP-1 can stimulate insulin secretion in HKO islets, although the magnitude was trending lower compared to WT [14].

Glycolysis-generated ATP binds to and closes K_{ATP} channels, resulting in membrane depolarization and activation of voltage-dependent calcium channels (VDCCs). Calcium influx through VDCCs induces fusion of insulin granules to the β-cell plasma membrane and insulin exocytosis. We investigated calcium flux in islets of various genotypes. Unlike triple FoxO knockout islets [3], membrane depolarization

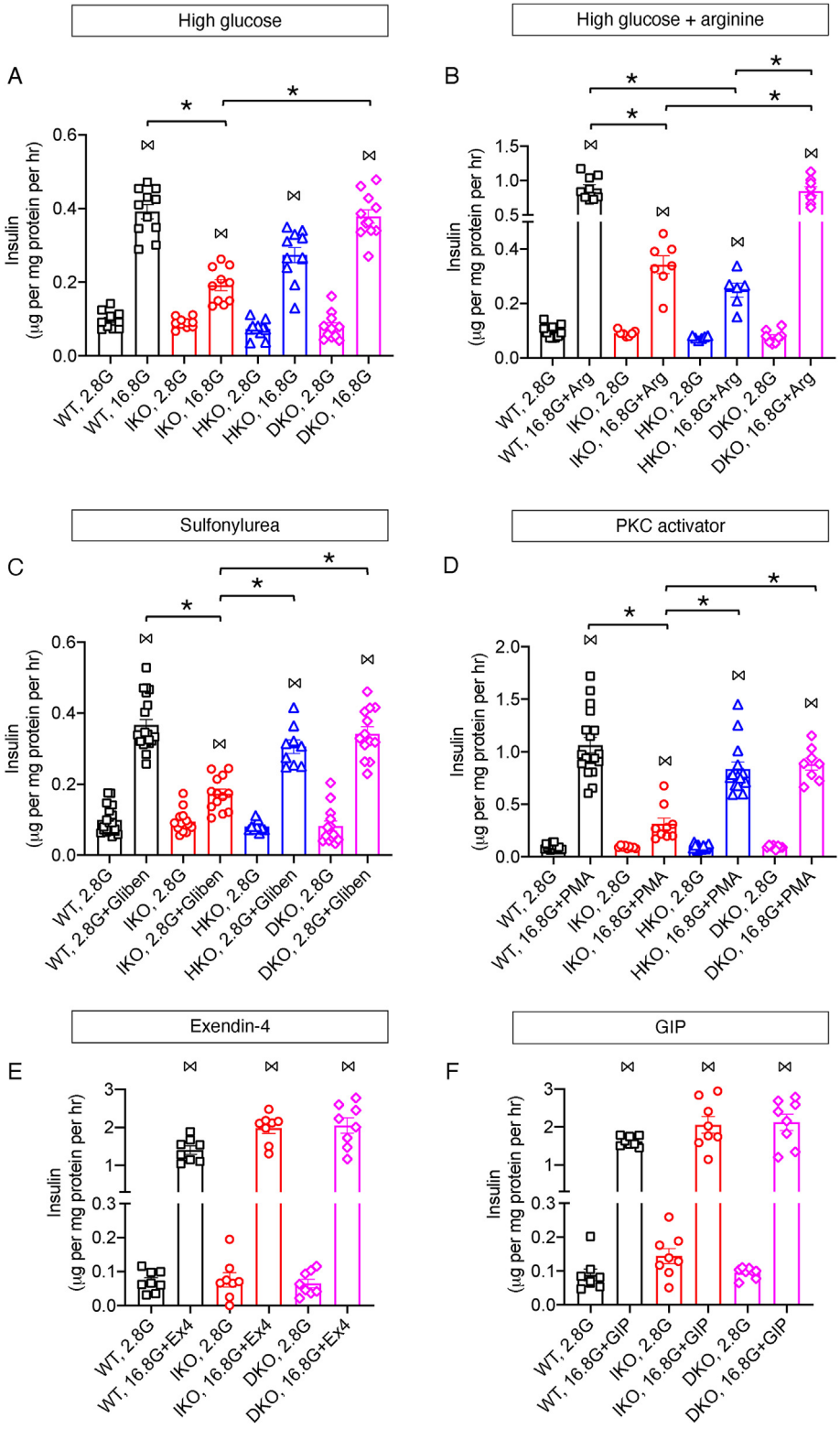

Figure 3: Ex vivo insulin secretion in purified islets. (A) High glucose-stimulated (16.8 mM or 16.8 G) insulin secretion in WT (n = 11), IKO (n = 10), HKO (n = 11), and DKO (n = 11) islets. (B) 16.8G and L-arginine-stimulated (10 mM or Arg) insulin secretion in WT (n = 10), IKO (n = 7), HKO (n = 6), and DKO (n = 8) islets. (C) Glibenclamide-stimulated (1 µM) insulin secretion in WT (n = 21), IKO (n = 14), HKO (n = 9), and DKO (n = 13) islets. (D) PMA-stimulated (1 µM) insulin secretion in WT (n = 18), IKO (n = 9), HKO (n = 14), and DKO (n = 8) islets. (E) Exendin-4-stimulated (Ex4, 1 µM) insulin secretion in WT (n = 8), IKO (n = 8), and DKO (n = 8) islets. (F) GIP-stimulated (1 µM) insulin secretion in WT (n = 8), IKO (n = 8), and DKO (n = 8) islets. Islets were first incubated in basal glucose (2.8 mM or 2.8G) followed by the indicated secretagogue(s). The results were normalized to the total protein content and duration of treatments. Error bars indicate SEM, ⋈ represents $p < 0.05$ when comparing basal glucose- and secretagogue-stimulated insulin secretion in the same genotype using Student's t-test, while * shows $p < 0.05$ when comparing secretagogue-stimulated insulin secretion in different genotypes using Student's t-test and ANOVA.

induced calcium influx in response to glucose and KCl was slightly increased in IKO (Figure 4A,B) [14]. Consistent with prior observations, HKO islets showed a decreased magnitude and a delayed onset of calcium influx compared to WT islets (Figure 4A,B). Interestingly, DKO restored the magnitude but not the delayed onset of calcium flux. As a result, the area under the curve of the calcium responses following glucose stimulation was restored by DKO at later but not earlier time points (Figure 4A, B). In summary, FoxO1 and Hnf4α affected insulin secretion in mechanistically distinct ways and resulted in antagonistic epistatic interactions.

3.4. Different mechanisms of β-cell dysfunction in FoxO1 vs Hnf4α mutants

To understand the mechanisms of epistasis between FoxO1 and Hnf4α, we introduced a fluorescent *ROSA26*-Tomato reporter in the various mutant strains and used it to sort genetically labeled Tomato-positive β-cells [8]. We performed RNAseq in WT, IKO, HKO, and DKO β-cells and identified expression changes by differential gene calling. Our working hypothesis was that functional antagonistic epistasis could result from: (i) synergistic regulation of networks that inhibit insulin secretion, (ii) antagonistic regulation of networks that promote insulin secretion, and (iii) mixed regulation of distinct components of individual networks (Figure 5) [15].

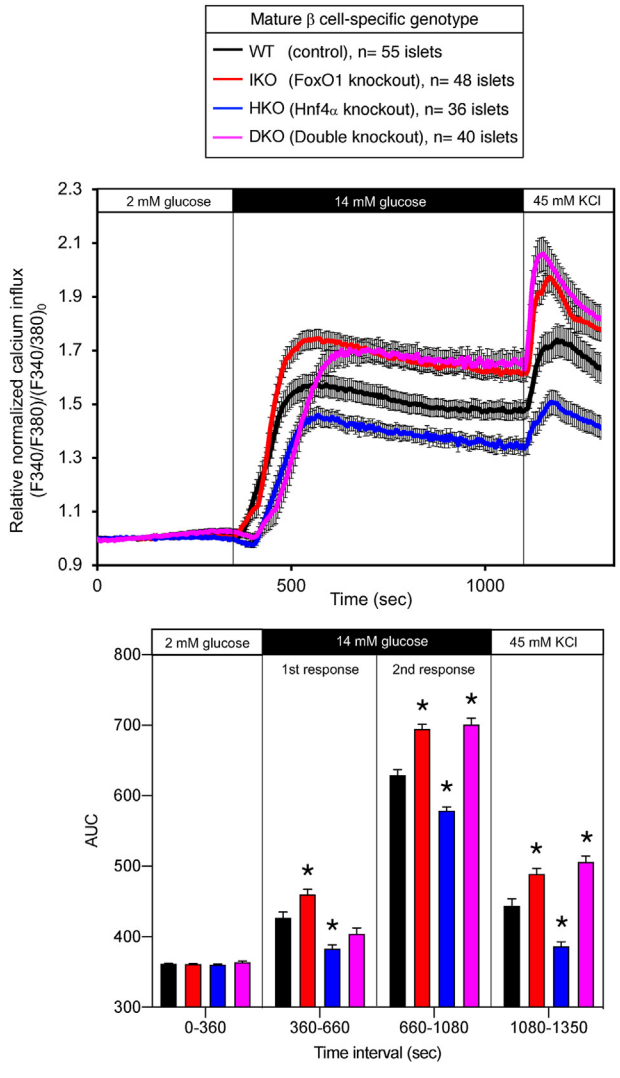

Figure 4: Average whole-islet calcium response. Islets were incubated for 20 min in 2 mM of glucose-containing solution and imaged using FURA2 prior to treatment with 14 mM of glucose. (A) Representative Fura-2 AM recordings (F340/F380) of changes in whole-islet intracellular calcium flux in WT, IKO, HKO, and DKO mice. The secretagogues employed are indicated on top. (B) Area under the curve (AUC) for different secretagogue-stimulated insulin secretion in A. Error bars indicate SEM, * represents $p < 0.05$ when comparing to WT using Student's t-test and ANOVA.

Compared to WT, there were changes to 769 mRNAs in IKO β-cells (Table S1), 1,327 in HKO (Table S2), and 1,692 in DKO (Table S3). Thus, the restoration of insulin secretion in DKO seemingly was not due to a normalization of gene expression but rather to the emergence of a distinct gene expression profile. This was confirmed by comparisons of single with double mutants, where DKO β-cells displayed 1,787 mRNA changes compared to IKO (Table S4) and 666 compared to HKO (Table S5). There were 1,165 mRNA changes between IKO and HKO β-cells (Table S6).

In IKO β-cells, we detected the expected alterations of known FoxO1 target mRNAs, with increased glycolytic genes [39], including β-cell "disallowed" genes [7] and *Aldh1a3* [36], as well as decreased *Cyb5r3* [40] (Table S1). These data were consistent with previous findings indicating that triple FoxO ablation results in altered metabolic coupling [3]. Specifically, the combination of increased glycolysis and impaired coupling to oxidative phosphorylation by activation of disallowed genes may result in lower efficiency of ATP production and increased ROS generation [41].

Previous reports differed with regard to gene expression patterns associated with Hnf4α deletion in β-cells [12,14]. In our cross, the most striking gene expression changes in HKO were the substantial increases in abundant mRNAs encoding mitochondrial cytochrome components (COX, CYTB, ND1, ND2, ND4, and ND5) (Table S2). Conversely, the mitochondrial complex III oxidoreductase *Cyb5r3* was decreased, possibly resulting in altered electron transport across the mitochondrial chain [40]. There were extensive increases in the family of KCN-type potassium channels, which may have affected membrane depolarization and insulin secretion, thus explaining the preserved response to sulfonylurea (Fig. S3A). Levels of L-type VDCC *Cacnb3* mRNA decreased, a finding that may partly explain the impaired calcium response in HKO islets (Table S2). Interestingly, this change was not reversed in DKO, consistent with the observation that first-phase calcium flux was not restored despite the overall improvement in calcium flux and insulin secretion (Table S3). These data indicated that the underlying mechanisms of islet dysfunction differed in IKO vs HKO islets. There were two notable exceptions to this: *Cyb5r3*, as previously indicated, and *Gpr119*, an orphan GPCR that is mechanistically linked to insulin secretion [42], were equally decreased in both IKO and HKO (Tables S1 and S2).

3.5. Epistatic network analysis

To examine whether the phenotypic epistasis between FoxO1 and Hnf4α was reflected in epistatic changes in gene expression, we averaged FPKM from five replicates of RNAseq for each genotype (WT, IKO, HKO, and DKO), normalized knockout to WT, and calculated an epistasis score using the following formula: epistasis (ε) = R observed (DKO) - R expected (IKO + HKO) [15]. Based on the distribution of the epistasis scores, we applied a cutoff of two standard deviations and assigned synergistic epistasis, non-epistasis, or antagonistic epistasis (Figure 5A and Table S7). We found 273 antagonistic genes and 59 synergistic genes whose gene ontology terms are shown in Figure S3A. These numbers indicated that the most common transcriptional epistasis between FoxO1 and Hnf4α was antagonistic.

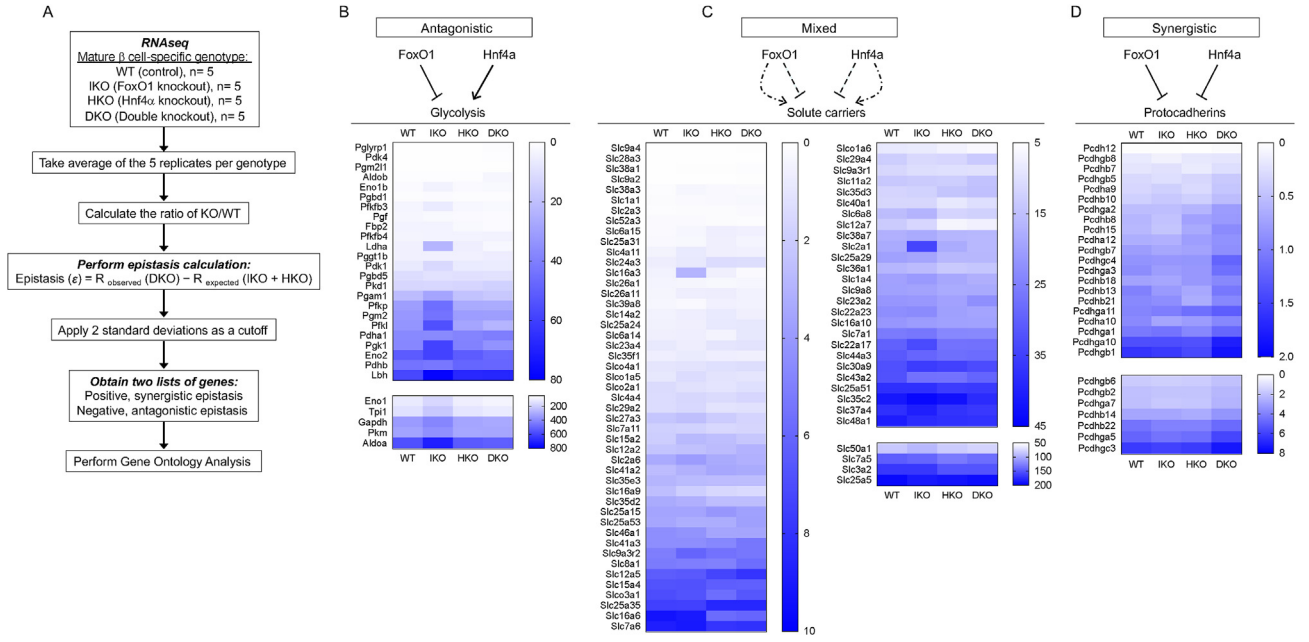

Figure 5: Epistatic modalities between FoxO1 and Hnf4α. (A) Workflow to determine the genetic epistasis between FoxO1 and Hnf4α. (B) Antagonistic epistasis-regulated glycolytic network. (C) Mixed epistasis for solute carrier lineage. (D) Synergistic epistasis-controlled protocadherins. Heatmaps demonstrate altered gene expression in DKO vs IKO or HKO β-cells. Scale bars indicate FPKM.

We recently showed that a key mediator of the effects of FoxO1 on insulin secretion is C2cd4a, a nuclear protein of unknown function with a potential role in repressing the expression of genes in the glycolytic cascade [7]. Indeed, key β-cell "disallowed" genes, such as *Ldha* (Figure 5B) and *Slc16a3* (Figure 5C), were substantially increased in IKO compared to WT. These changes were reversed in DKO. The predicted outcome of this reversal would be (i) a decrease in glucose utilization to promote β-cell resting, which reduces the levels of glucose toxicity-generated reactive oxygen species (ROS), (ii) tighter coupling of glycolysis with oxidative phosphorylation due to reduced *Ldha* activity, and (iii) strictly maintained glucose- but not lactate- or pyruvate-induced insulin secretion through repressing monocarboxylate transporter. This change in glucose utilization was consistent with antagonistic epistasis of FoxO1 and Hnf4α on the glycolytic cascade, with the former acting as a suppressor and the latter as an activator of this pathway (Figure 5B).

In contrast, changes to HKO gene expression patterns were not reversed in either WT or DKO islets. For example, the patterns of KCN expression remained virtually identical (Fig. S3B). Even when analyzing the vast and heterogenous family of solute carriers (*Slc*), 61% of the changes seen in HKO failed to be reversed as opposed to 23% in IKO islets. Thus, the majority of Hnf4α targets were not epistatic with FoxO1.

Notably, a remarkable synergistic regulation of the protocadherin gene family emerged by comparing HKO with WT or DKO islets (Figure 5D). Gene ontology analysis of synergistic epistatic genes was also consistent with this finding (Fig. S3C). Protocadherins are thought to participate in the formation of adherens (tight) junctions between β-cells that facilitate calcium influx and fusion of secretory vesicles [43]. This may explain the unique patterns of calcium entry into DKO islets, which were slower but reached higher levels than WT. This regulation of the protocadherin family was consistent with a model of synergistic epistasis. In this instance, both FoxO1 and Hnf4α acted in a similar fashion to repress expression of these genes, and it was only when both were removed that the full extent of the regulation became apparent.

4. DISCUSSION

β-Cell function is maintained through a restricted network of transcription factors [44]. However, the redundancy, heterogeneity, and complexity of gene expression patterns associated with experimental or naturally occurring perturbations in the activity of these "master" regulators complicate the task of interrogating the mechanisms of dysfunction resulting from their interactions. The main findings of this work are: (i) FoxO1 deletion resulted in an enrichment of Hnf4α motifs in FoxO1 distal enhancers in β-cells, (ii) this enrichment was associated with an antagonistic phenotypic epistasis (opposite effects on insulin secretion) and gene expression epistasis between these transcription factors (273 antagonistic genes vs 59 synergistic genes), (iii) compounded deletion of FoxO1 and Hnf4α reversed the phenotype of reduced insulin secretion in single knockouts, and (iv) gene expression analyses revealed that the restored phenotype in double knockout mice was not due to a simple reversal of the RNA profile to WT, but to different epistatic modalities regulating different networks. Examples include antagonistic epistasis of the glycolysis pathway, and synergistic epistasis of the protocadherin gene family. Epistatic synergism between paralogues in β-cell function has been proposed [13]. But antagonistic epistasis between distinct factors possibly acting through cis-acting enhancers and resulting in mechanistically distinct phenotypes had not been disclosed.

The interaction between FoxO1 and Hnf4α occurs at multiple levels. The two proteins physically interact in the liver [45]. In addition, Hnf4α-initiated glucokinase transcription is repressed by FoxO1 acting as a co-repressor [46,47] via SIN3a [48]. However, the co-regulation of pancreatic β-cell distal enhancers by FoxO1 and Hnf4α has not been revealed until now, and its relevance to the progression of common forms of diabetes in humans will have to be further explored.

Type 2 diabetes is a polygenic disease, and β-cell failure has acquired and genetic components. FoxO1 can be considered an example of the former and Hnf4α of the latter. Both homozygous null mutations in β-

cells are associated with an insulin secretory defect, although the mechanisms appear to differ. Thus, the absent sulfonylurea response in FoxO1 knockout mice was reminiscent of the acquired failure seen in diabetic patients, while Hnf4α knockout showed a preserved sulfonylurea response similar to MODY1 patients [11]. The extent to which the recently characterized Foxo1 target Cyb5r3 was responsible for some of the impairment of insulin secretion seen herein is currently under investigation by our laboratory [40]. The calcium response to glucose differed in the FoxO1 and Hnf4α single mutants, although this may partly be explained by the compensatory function of FoxO3 in single FoxO1 knockouts [3]. When considering the difference in the calcium response in FoxO1 single knockout mice in this study vs FoxO1, 3a, and 4 triple knockout mice [3], the increased calcium influx in FoxO1 single knockouts was reminiscent of the excitotoxicity seen, for example, in Abcc8 knockout β-cells with persistent membrane depolarization, elevated intracellular calcium, and increased expression of the β-cell dedifferentiation marker, Aldh1a3 [49]. Of note, the ages of the mice used also differed, with the FoxO1 single knockout mice in the current study being 6–8 months old, while FoxO1, 3a, and 4 triple knockout mice were 3–4 months old. Thus, it was possible that the excitotoxicity (single knockouts) predated decreased calcium influx (triple knockouts).

Evidence of antagonistic epistasis between these factors arose from the surprising phenotype of the double mutant mice. However, the majority of Hnf4α-dependent changes were unaffected by the FoxO1 mutation, indicating that epistasis between these two proteins occurred primarily within the FoxO1 regulome. For example, the Hnf1α network was inhibited in the HKO mutants (data not shown), and this alteration was not rescued in the DKO mice. Conversely, most changes induced by FoxO1 ablation appeared to be offset by the Hnf4α mutation. The most striking example was the antagonistic regulation of glycolysis, where FoxO1 acted as a suppressor and Hnf4α as an activator of gene expression. Although the association of reduced expression of glycolytic genes with restored insulin secretion in DKO islets may appear counter-intuitive, it includes suppression of *Ldha*, and therefore can be conducive to better metabolic coupling of glycolysis with mitochondrial oxidative phosphorylation, leading to β-cell resting and reduced ROS production [41].

A second example of the epistatic network was represented by the synergistic suppression of protocadherins. The release of this suppression in the DKO mice may have led to tighter coupling of neighboring β-cells and therefore faster propagation of action potentials, reducing heterogeneity among β-cells [43]. Consistent with this hypothesis was the observation that calcium influx into DKO occurred even more rapidly than in WT β-cells. While further studies will be required to investigate this mechanism, these observations raise the possibility that agents that improve cell–cell communication can restore insulin secretion in diabetes.

In summary, our findings of distinct and functionally competing roles of Hnf4α and FoxO1 contributory to β-cell dysfunction highlighted the role of antagonistic epistasis between transcription factors in the maintenance of pancreatic β-cells. To the extent that the two factors represent genetic (Hnf4α) and acquired abnormalities (FoxO1) of gene expression, these findings can provide a model to understand the pathophysiology of β-cell dysfunction.

AUTHOR CONTRIBUTIONS

Conceptualization: T.K. and D.A. Methodology: T.K. and D.A. Investigation: T.K., W.D., Y.M., and P.K.D. Formal analysis: T.K., W.D., Y.M., P.K.D., D.A.J., D.S., and D.A. Writing original draft: T.K. and D.A. Writing, review, and editing T.K., W.D., Y.M., P.K.D., D.A.J., D.S., and D.A. Funding acquisition: T.K., D.A.J., and D.A.

FUNDING

This study was supported by NIH grants T32DK07328 (to T.K.), K01DK114372 (to T.K.), DK097392 (to D.A.J.), DK115620 (to D.A.J.), DK64819 (to D.A.), DK63608 (to Columbia University Diabetes Research Center), and the JPB Foundation (to D.A. and Mitchell A. Lazar).

ACKNOWLEDGMENTS

We give special thanks to Mitchell A. Lazar (University of Pennsylvania) and Manashree Damle (Massachusetts General Hospital) for their bioinformatics support and guidance. We also thank members of the Accili laboratory for discussions and Thomas Kolar, Ana Flete-Castro, and Qiong Xu (Columbia University) for technical support. Dr. Taiyi Kuo was this study's guarantor and as such had full access to all of the data and takes responsibility for the data integrity and accuracy of the data analysis.

CONFLICTS OF INTEREST

No potential conflicts of interest relevant to this article were reported. Dr. Accili is founder and director of Forkhead Biotherapeutics and is required by his institution to state so in his publications.

APPENDIX A. SUPPLEMENTARY DATA

Supplementary data to this article can be found online at https://doi.org/10.1016/j.molmet.2021.101256.

REFERENCES

[1] Ferrannini, E., 2010. The stunned beta cell: a brief history. Cell Metabolism 11: 349–352.
[2] Fajans, S.S., Bell, G.I., 2011. MODY: history, genetics, pathophysiology, and clinical decision making. Diabetes Care 34:1878–1884.
[3] Kim-Muller, J.Y., Zhao, S., Srivastava, S., Mugabo, Y., Noh, H.L., Kim, Y.R., et al., 2014. Metabolic inflexibility impairs insulin secretion and results in MODY-like diabetes in triple FoxO-deficient mice. Cell Metabolism 20:593–602.
[4] Talchai, C., Xuan, S., Lin, H.V., Sussel, L., Accili, D., 2012. Pancreatic beta cell dedifferentiation as a mechanism of diabetic beta cell failure. Cell 150:1223–1234.
[5] Cinti, F., Bouchi, R., Kim-Muller, J.Y., Ohmura, Y., Sandoval, P.R., Masini, M., et al., 2016. Evidence of beta-cell dedifferentiation in human type 2 diabetes. The Journal of Cinical Endocrinology and Metabolism 101:1044–1054.
[6] Sun, J., Ni, Q., Xie, J., Xu, M., Zhang, J., Kuang, J., et al., 2019. Beta-cell dedifferentiation in patients with T2D with adequate glucose control and nondiabetic chronic pancreatitis. The Journal of Cinical Endocrinology and Metabolism 104:83–94.
[7] Kuo, T., Kraakman, M.J., Damle, M., Gill, R., Lazar, M.A., Accili, D., 2019. Identification of C2CD4A as a human diabetes susceptibility gene with a role in beta cell insulin secretion. Proceedings of the National Academy of Sciences of the United States of America 116:20033–20042.
[8] Kuo, T., Damle, M., Gonzalez, B.J., Egli, D., Lazar, M.A., Accili, D., 2019. Induction of alpha cell-restricted Gc in dedifferentiating beta cells contributes to stress-induced beta-cell dysfunction. JCI Insight 5.
[9] Yamagata, K., Furuta, H., Oda, N., Kaisaki, P.J., Menzel, S., Cox, N.J., et al., 1996. Mutations in the hepatocyte nuclear factor-4alpha gene in maturity-onset diabetes of the young (MODY1). Nature 384:458–460.

[10] Herman, W.H., Fajans, S.S., Ortiz, F.J., Smith, M.J., Sturis, J., Bell, G.I., et al., 1994. Abnormal insulin secretion, not insulin resistance, is the genetic or primary defect of MODY in the RW pedigree. Diabetes 43:40–46.
[11] Gardner, D.S., Tai, E.S., 2012. Clinical features and treatment of maturity onset diabetes of the young (MODY). Diabetes Metab Syndr Obes 5:101–108.
[12] Gupta, R.K., Vatamaniuk, M.Z., Lee, C.S., Flaschen, R.C., Fulmer, J.T., Matschinsky, F.M., et al., 2005. The MODY1 gene HNF-4alpha regulates selected genes involved in insulin secretion. Journal of Clinical Investigation 115:1006–1015.
[13] Boj, S.F., Petrov, D., Ferrer, J., 2010. Epistasis of transcriptomes reveals synergism between transcriptional activators Hnf1alpha and Hnf4alpha. PLoS Genetics 6:e1000970.
[14] Miura, A., Yamagata, K., Kakei, M., Hatakeyama, H., Takahashi, N., Fukui, K., et al., 2006. Hepatocyte nuclear factor-4alpha is essential for glucose-stimulated insulin secretion by pancreatic beta-cells. Journal of Biological Chemistry 281:5246–5257.
[15] Snitkin, E.S., Segre, D., 2011. Epistatic interaction maps relative to multiple metabolic phenotypes. PLoS Genetics 7:e1001294.
[16] Kuo, T., Kim-Muller, J.Y., McGraw, T.E., Accili, D., 2016. Altered plasma profile of antioxidant proteins as an early correlate of pancreatic beta cell dysfunction. Journal of Biological Chemistry 291:9648–9656.
[17] Kuo, T., Lew, M.J., Mayba, O., Harris, C.A., Speed, T.P., Wang, J.C., 2012. Genome-wide analysis of glucocorticoid receptor-binding sites in myotubes identifies gene networks modulating insulin signaling. Proceedings of the National Academy of Sciences of the United States of America 109:11160–11165.
[18] Li, H., Durbin, R., 2009. Fast and accurate short read alignment with Burrows-Wheeler transform. Bioinformatics 25:1754–1760.
[19] Zhang, Y., Liu, T., Meyer, C.A., Eeckhoute, J., Johnson, D.S., Bernstein, B.E., et al., 2008. Model-based analysis of ChIP-seq (MACS). Genome Biology 9:R137.
[20] Whyte, W.A., Orlando, D.A., Hnisz, D., Abraham, B.J., Lin, C.Y., Kagey, M.H., et al., 2013. Master transcription factors and mediator establish super-enhancers at key cell identity genes. Cell 153:307–319.
[21] Kuo, T., Chen, T.C., Yan, S., Foo, F., Ching, C., McQueen, A., et al., 2014. Repression of glucocorticoid-stimulated angiopoietin-like 4 gene transcription by insulin. The Journal of Lipid Research 55:919–928.
[22] Dobin, A., Davis, C.A., Schlesinger, F., Drenkow, J., Zaleski, C., Jha, S., et al., 2013. STAR: ultrafast universal RNA-seq aligner. Bioinformatics 29:15–21.
[23] Liao, Y., Smyth, G.K., Shi, W., 2014. featureCounts: an efficient general purpose program for assigning sequence reads to genomic features. Bioinformatics 30:923–930.
[24] Love, M.I., Huber, W., Anders, S., 2014. Moderated estimation of fold change and dispersion for RNA-seq data with DESeq2. Genome Biology 15:550.
[25] Dickerson, M.T., Bogart, A.M., Altman, M.K., Milian, S.C., Jordan, K.L., Dadi, P.K., et al., 2018. Cytokine-mediated changes in K(+) channel activity promotes an adaptive Ca(2+) response that sustains beta-cell insulin secretion during inflammation. Scientific Reports 8:1158.
[26] Creyghton, M.P., Cheng, A.W., Welstead, G.G., Kooistra, T., Carey, B.W., Steine, E.J., et al., 2010. Histone H3K27ac separates active from poised enhancers and predicts developmental state. Proceedings of the National Academy of Sciences of the United States of America 107:21931–21936.
[27] Lenhard, B., Sandelin, A., Carninci, P., 2012. Metazoan promoters: emerging characteristics and insights into transcriptional regulation. Nature Reviews Genetics 13:233–245.
[28] Kitamura, T., Kitamura, Y.I., Kobayashi, M., Kikuchi, O., Sasaki, T., Depinho, R.A., et al., 2009. Regulation of pancreatic juxtaductal endocrine cell formation by FoxO1. Molecular and Cellular Biology 29:4417–4430.
[29] Kim-Muller, J.Y., Kim, Y.J., Fan, J., Zhao, S., Banks, A.S., Prentki, M., et al., 2016. FoxO1 deacetylation decreases fatty acid oxidation in beta-cells and sustains insulin secretion in diabetes. Journal of Biological Chemistry 291:10162–10172.
[30] Sander, M., Neubuser, A., Kalamaras, J., Ee, H.C., Martin, G.R., German, M.S., 1997. Genetic analysis reveals that PAX6 is required for normal transcription of pancreatic hormone genes and islet development. Genes & Development 11:1662–1673.
[31] Hart, A.W., Mella, S., Mendrychowski, J., van Heyningen, V., Kleinjan, D.A., 2013. The developmental regulator Pax6 is essential for maintenance of islet cell function in the adult mouse pancreas. PloS One 8:e54173.
[32] Swisa, A., Avrahami, D., Eden, N., Zhang, J., Feleke, E., Dahan, T., et al., 2017. PAX6 maintains beta cell identity by repressing genes of alternative islet cell types. Journal of Clinical Investigation 127:230–243.
[33] Liu, H.L., Yang, H.Y., Liu, L.X., Chen, Y., Kuang, H.Y., Zhang, H.J., et al., 2011. Relationship between down-regulation of HIC1 and PTEN genes and dysfunction of pancreatic islet cells in diabetic rats. Acta Histochemica 113:340–348.
[34] Luo, Y., He, F., Hu, L., Hai, L., Huang, M., Xu, Z., et al., 2014. Transcription factor Ets1 regulates expression of thioredoxin-interacting protein and inhibits insulin secretion in pancreatic beta-cells. PloS One 9:e99049.
[35] Chen, F., Sha, M., Wang, Y., Wu, T., Shan, W., Liu, J., et al., 2016. Transcription factor Ets-1 links glucotoxicity to pancreatic beta cell dysfunction through inhibiting PDX-1 expression in rodent models. Diabetologia 59:316–324.
[36] Kim-Muller, J.Y., Fan, J., Kim, Y.J., Lee, S.A., Ishida, E., Blaner, W.S., et al., 2016. Aldehyde dehydrogenase 1a3 defines a subset of failing pancreatic beta cells in diabetic mice. Nature Communications 7:12631.
[37] Herrera, P.L., 2000. Adult insulin- and glucagon-producing cells differentiate from two independent cell lineages. Development 127:2317–2322.
[38] Brouwers, B., de Faudeur, G., Osipovich, A.B., Goyvaerts, L., Lemaire, K., Boesmans, L., et al., 2014. Impaired islet function in commonly used transgenic mouse lines due to human growth hormone minigene expression. Cell Metabolism 20:979–990.
[39] Buteau, J., Shlien, A., Foisy, S., Accili, D., 2007. Metabolic diapause in pancreatic beta-cells expressing a gain-of-function mutant of the forkhead protein Foxo1. Journal of Biological Chemistry 282:287–293.
[40] Fan, J., Du, W., Kim-Muller, J.Y., Son, J., Kuo, T., Larrea, D., et al., 2020. Cyb5r3 links FoxO1-dependent mitochondrial dysfunction with beta-cell failure. Molecular metabolism 34:97–111.
[41] Robertson, R.P., Harmon, J., Tran, P.O., Tanaka, Y., Takahashi, H., 2003. Glucose toxicity in beta-cells: type 2 diabetes, good radicals gone bad, and the glutathione connection. Diabetes 52:581–587.
[42] Abdel-Magid, A.F., 2019. Treatment of diabetes, obesity, dyslipidemia, and related disorders with GPR119 agonists. ACS Medicinal Chemistry Letters 10:14–15.
[43] Dissanayake, W.C., Sorrenson, B., Shepherd, P.R., 2018. The role of adherens junction proteins in the regulation of insulin secretion. Bioscience Reports 38.
[44] Fujitani, Y., 2017. Transcriptional regulation of pancreas development and beta-cell function [Review]. Endocrine Journal 64:477–486.
[45] Puigserver, P., Rhee, J., Donovan, J., Walkey, C.J., Yoon, J.C., Oriente, F., et al., 2003. Insulin-regulated hepatic gluconeogenesis through FOXO1-PGC-1alpha interaction. Nature 423:550–555.
[46] Hirota, K., Sakamaki, J., Ishida, J., Shimamoto, Y., Nishihara, S., Kodama, N., et al., 2008. A combination of HNF-4 and Foxo1 is required for reciprocal transcriptional regulation of glucokinase and glucose-6-phosphatase genes in response to fasting and feeding. Journal of Biological Chemistry 283:32432–32441.
[47] Ganjam, G.K., Dimova, E.Y., Unterman, T.G., Kietzmann, T., 2009. FoxO1 and HNF-4 are involved in regulation of hepatic glucokinase gene expression by resveratrol. Journal of Biological Chemistry 284:30783–30797.
[48] Langlet, F., Haeusler, R.A., Linden, D., Ericson, E., Norris, T., Johansson, A., et al., 2017. Selective inhibition of FOXO1 activator/repressor balance modulates hepatic glucose handling. Cell 171:824–835 e818.
[49] Stancill, J.S., Cartailler, J.P., Clayton, H.W., O'Connor, J.T., Dickerson, M.T., Dadi, P.K., et al., 2017. Chronic beta-cell depolarization impairs beta-cell identity by disrupting a network of Ca(2+)-regulated genes. Diabetes 66:2175–2187.

